Published in Physical Review A 69, issue 063403, 1-9, 2004
which should be used for any reference to this work

Laser collimation of a continuous beam of cold atoms using Zeeman-shift degenerate-Raman-sideband cooling

G. Di Domenico,* N. Castagna, G. Mileti, and P. Thomann
Observatoire cantonal, rue de l'Observatoire 58, 2000 Neuchâtel, Switzerland

A. V. Taichenachev and V. I. Yudin
Novosibirsk State University, Pirogova 2, Novosibirsk 630090, Russia
Institute of Laser Physics SB RAS, Lavrent'eva 13/3, Novosibirsk 630090, Russia

In this article we report on the use of degenerate-Raman-sideband cooling for the collimation of a continuous beam of cold cesium atoms in a fountain geometry. Thanks to this powerful cooling technique we have reduced the atomic beam transverse temperature from 60 μK to 1.6 μK in a few milliseconds. The longitudinal temperature of 80 μK is not modified. The flux density, measured after a parabolic flight of 0.57 s, has been increased by a factor of 4 to approximately 10^7 at. s^{-1} cm^{-2} and we have identified a Sisyphus-like precooling mechanism which should make it possible to increase this flux density by an order of magnitude.

I. INTRODUCTION

Since the discovery of laser cooling [1], beams of slow and cold atoms have played an ever more important role in high-precision experiments—e.g., in atomic interferometry experiments [2,3] and atomic fountain clocks [4]. In this context the continuous beam approach [5] is interesting because it dramatically reduces all undesirable effects of atomic density [4] and the Dick effect which is unavoidable in pulsed beams [6,7]. However, to take full advantage of the continuous beam approach, one needs to increase the useful flux. One method is to collimate the atomic beam.

In this paper we present a laser cooling experiment for the collimation of a continuous beam of cold cesium atoms in a fountain geometry. The technique that we use is Zeeman-shift degenerate-Raman-sideband cooling. Sideband cooling was first applied to trapped ions [8–10]. Later, following a theoretical proposal by Taïeb *et al.* [11], it was adapted to neutral atoms in optical lattices by several groups [12–14]. Recently, the group of Chu developed a particularly efficient scheme [15] for three-dimensional (3D) cooling of a pulsed cesium beam [16]. Here we report on a demonstration of this mechanism for two-dimensional cooling of a continuous atomic beam.

II. DEGENERATE-RAMAN-SIDEBAND COOLING PRINCIPLE

The cooling scheme we use is similar to that proposed by Chu and co-workers [15,16]. Let us briefly recall its principle. Cesium atoms are trapped in a far-off-resonance optical lattice and their center-of-mass motion is quantized. In this context we cool the atoms with a succession of cycles, decreasing their vibrational energy level n until they reach the ground state $n=0$. As depicted in Fig. 1, for $n>1$, each cycle consists of two Raman transitions $|F=3, m_F=3, n\rangle \rightarrow |3, 2, n-1\rangle \rightarrow |3, 1, n-2\rangle$ followed by an optical pumping cycle towards $|3, 3, n-2\rangle$. Each Raman transition removes one vibrational quantum but the optical pumping conserves n with high probability because the atoms are in the Lamb-Dicke regime. Notice that for $n=1$ we need a cycle made up of only one Raman transition $|F=3, m_F=3, n=1\rangle \rightarrow |3, 2, 0\rangle$ followed by optical pumping to bring the atom to the ground state $|3,3,0\rangle$. The Raman cooling process ends

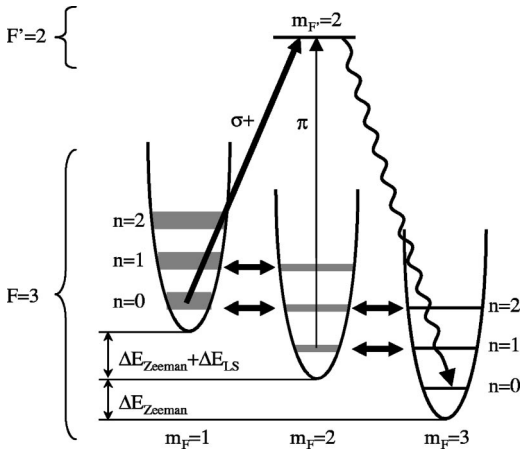

FIG. 1. Degenerate-Raman-sideband cooling scheme adapted from [15] by permission of the authors. Atoms trapped in optical potential wells are brought to the vibrational ground state $n=0$ by a sequence of cooling cycles. Each cycle is composed of two Raman transitions (double arrows) followed by fast σ^+ optical pumping except the last cycle which is composed of a single Raman transition followed by slow π pumping (fast and slow are relative to the Raman transition rate). Cooling ends in the state $|F=3, m_F=3, n=0\rangle$ which is dark for both pumping and lattice laser. Different vibrational levels are brought into degeneracy using a magnetic field ($\Delta E_{\mathrm{Zeeman}}$). The strong σ^+ pumping beam induces a light shift on $m_F=1$ sublevels (ΔE_{LS}). Fortunately, it also broadens these $m_F=1$ sublevels, which helps to preserve the degeneracy.

*Electronic address: Gianni.DiDomenico@ne.ch

there since the ground state is dark to both the lattice and pumper beams. One can further cool the atoms by adiabatic expansion of the potential well as in Ref. [17].

Two lasers are needed to realize this cooling scheme. First, for the optical lattice, we need a high-power laser far detuned to the red of the $F=3\rightarrow F'=2,3,4$ transitions of the cesium D_2 line. By tuning this laser to the $F=4\rightarrow F'=3$ or $F=4\rightarrow F'=4$ transition we obtain a detuning of $\Delta=-2\pi\times 9$ GHz and the laser acts simultaneously as a repumper towards the $F=3$ hyperfine ground state. Second, to complete the cooling cycle, we need an optical pumping laser tuned in the neighborhood of the $F=3\rightarrow F'=2$ transition of the D_2 line. This laser should be mostly σ^+ to favor cycles with two Raman transitions but it should also contain a small π component for the last cooling cycle. Degenerate Raman transitions can be stimulated by the optical lattice laser itself. By a proper choice of polarizations, Raman couplings can be induced between the states $|F=3,\ m_F=3,\ n\rangle$ and $|3,\ 2,\ n-1\rangle$ brought into degeneracy by a magnetic field, as well as between $|3,\ 2,\ n-1\rangle$ and $|3,\ 1,\ n-2\rangle$.

Typical cooling times are a few milliseconds and the atomic beam crosses the cooling zone with a velocity of approximately 3 m/s. Therefore cooling can be achieved in a continuous mode with laser beams a few millimeters in diameter. In comparison with previous work [12,15,16] our experiment has the following distinctive features. We operate sideband cooling in continuous mode on an atomic beam. The initial temperature as given by our continuous cold atom source (60 μK) is much higher than that of sequential experiments (2–3 μK) [12,15,16]. The lattice potential depth seen by the atoms when crossing the collimation zone is not constant (because of Gaussian laser beams). We use a 2D optical lattice which combines symmetry, phase stability, and power recycling. See Sec. IV for details.

III. OPTICAL LATTICE

The field configuration used for the optical lattice consists of four linearly polarized beams having equal amplitudes and propagating in the xy plane along the x and y axes. The resulting field can be written as

$$\mathbf{E}(\mathbf{r},t)=E_0\mathcal{E}(\mathbf{r})\exp(-i\omega_L t)+\text{c.c.}, \tag{1}$$

$$\mathcal{E}(\mathbf{r})=\mathbf{n}_1\exp(iky)+\mathbf{n}_2\exp(-iky)+\mathbf{n}_3\exp(-ikx)+\mathbf{n}_4\exp(ikx),$$

where E_0 is the single-beam amplitude and $\mathbf{n}_i$ is the unit polarization vector of the ith beam. All the beams have the same frequency ω_L, far-detuned to the red of transitions $F=3\rightarrow F'=2,3,4$ of the D_2 resonance line. The lattice field induces spatially nonuniform optical shifts of substates with total angular momentum $F=3$. As was shown in Ref. [18], if the detuning is much greater than the hyperfine splitting of the excited state, the optical potential for the ground state takes the form

$$\hat{U}=-\frac{2}{3}u_s|\mathcal{E}(\mathbf{r})|^2-\frac{i}{12}u_s[\mathcal{E}(\mathbf{r})^*\times\mathcal{E}(\mathbf{r})]\cdot\hat{\mathbf{F}}. \tag{2}$$

Here $\hat{\mathbf{F}}$ is the angular momentum operator; the single-beam light shift $u_s=-AI/\Delta$ is proportional to the single-beam light intensity I and inversely proportional to the detuning $\Delta=\omega_L-\omega_{F,F'_{\max}}$. The constant A is given by $A=\hbar\Gamma^2/(8I_s)$ where $\Gamma=2\pi\times 5.3$ MHz is the natural width of the transition and $I_s=1.1$ mW cm^{-2} is the saturation intensity. The first term in Eq. (2) describes an isotropic energy shift (the same for all Zeeman sublevels) proportional to the energy density of the field. The second term acts as an effective magnetic field with magnitude and direction governed by the vector $i[\mathcal{E}(\mathbf{r})^*\times\mathcal{E}(\mathbf{r})]$. In general, the relationship between the scalar and vector terms in the optical shift operator is governed by the beam polarizations $\mathbf{n}_i$—i.e., by the orientation angles α and β of the wave plates in the present setup: see Fig. 3. For the field configuration considered here ($\alpha=\pi/8$ and $\beta=0$) we have

$$w(x,y)=|\mathcal{E}(\mathbf{r})|^2=4[1+\cos(kx)\cos(ky)], \tag{3}$$

$$\mathbf{M}(x,y)=i[\mathcal{E}(\mathbf{r})^*\times\mathcal{E}(\mathbf{r})]=4[\mathbf{e}_x\sin(kx)+\mathbf{e}_y\sin(ky)]\times[\cos(kx)+\cos(ky)]. \tag{4}$$

These scalar w and vector $\mathbf{M}$ are shown in Fig. 2. When the local quantization axis is chosen along the vector $\mathbf{M}(x,y)$, the optical shift operator $\hat{U}$ is diagonal. The corresponding eigenvalues (adiabatic potentials) are written as

$$U_m(x,y)=-\frac{2}{3}u_s w(x,y)+\frac{m_F}{12}u_s|\mathbf{M}(x,y)|, \tag{5}$$

where $m_F=-F,\ldots,F$ enumerates adiabatic states. However, if we choose the quantization axis along the static magnetic field $\mathbf{B}$, which is antiparallel with Oy (see Fig. 3), the diagonal part of the optical shift operator,

$$\hat{U}^{(\text{diag})}=-\frac{2}{3}u_s w(x,y)-\frac{1}{3}u_s\sin(ky)[\cos(kx)+\cos(ky)]\hat{F}_y, \tag{6}$$

defines m_F-dependent anisotropic potentials. The transverse off-diagonal term

$$\hat{U}^{(R)}=-\frac{1}{3}u_s\sin(kx)[\cos(kx)+\cos(ky)]\hat{F}_x \tag{7}$$

induces the Raman transitions between vibrational manifolds of adjacent Zeeman substates. These Zeeman sublevels are shifted due to both the static magnetic field and optical pumping field. The resonant Raman transitions are shown in Fig. 1. It is worth noting that in the strong Raman coupling regime the off-resonant Raman transitions should be taken into account as well.

We calculate the vibrational frequencies ω_v using the harmonic approximation of the diagonal elements of $\hat{U}^{(\text{diag})}$ from Eq. (6). As a numerical example, we take $I=100$ mW cm^{-2} and $\Delta=-2\pi\times 9$ GHz. Then $\hbar^{-1}u_s\approx 2\pi$

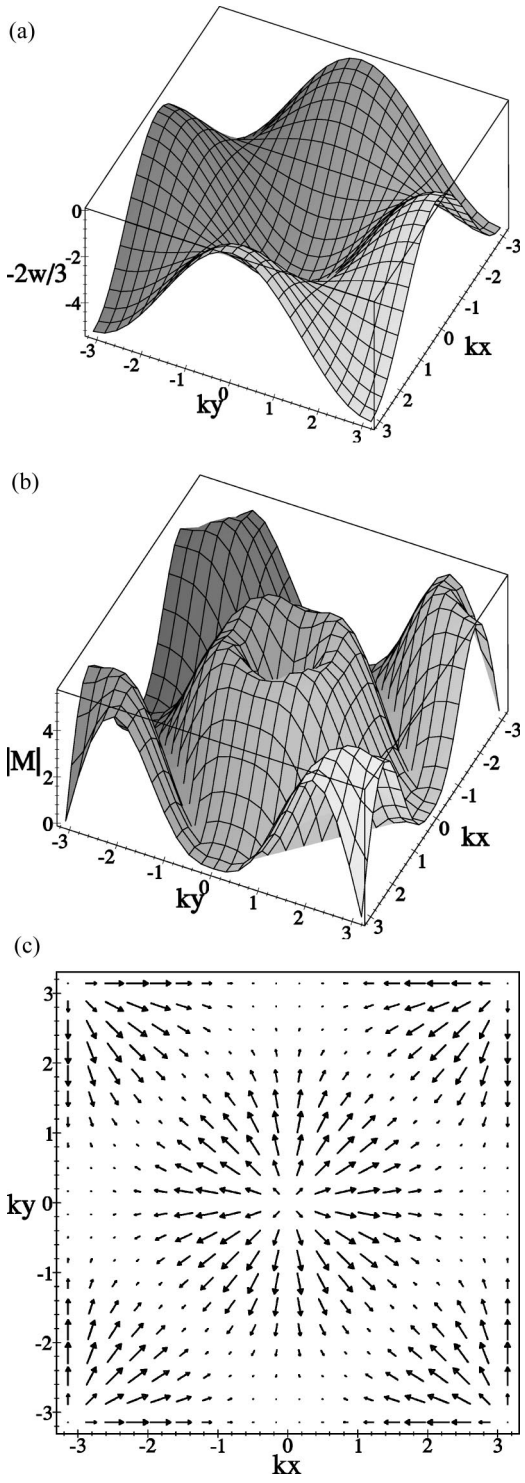

FIG. 2. Spatial dependence of the optical potential operator $\hat{U}(x,y)$, from Eq. (2), within one potential well, $-\pi<kx<+\pi$ and $-\pi<ky<+\pi$. (a) Plot of the dimensionless scalar potential $-\frac{2}{3}w(x,y)$, from Eq. (3), as a function of kx and ky. (b) Plot of the dimensionless absolute value of the vector $\mathbf{M}(x,y)$, from Eq. (4), as a function of kx and ky. (c) Plot of the directions of the vector $\mathbf{M}(x,y)$, from Eq. (4), as a function of kx and ky. Note that the vector part $\mathbf{M}(x,y)$ is odd with respect to the origin, which provides the Raman coupling between adjacent vibrational levels.

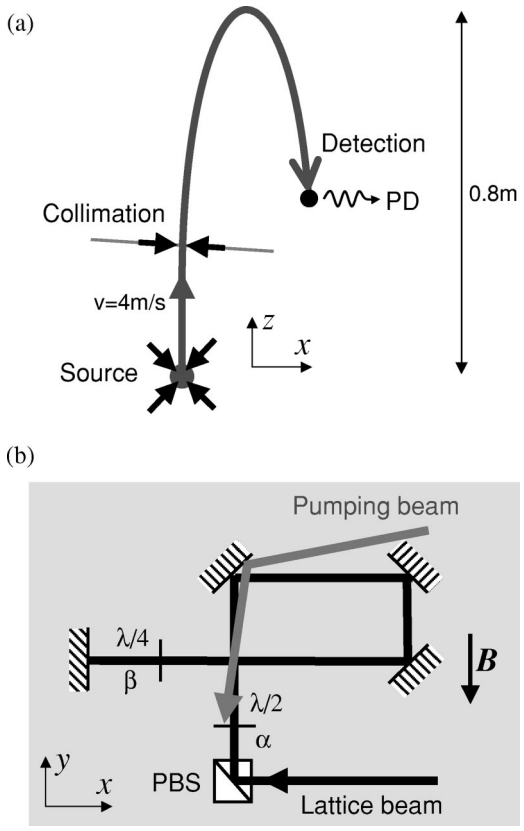

FIG. 3. Scheme of the experiment. (a) Vertical plane. The source of the continuous beam of cold atoms is a six beam moving molasses, four of which are shown. It is described in details in Ref. [20]. The collimation plane is tilted at about 3° to the horizontal in such a way that the atoms arrive at detection after a parabolic flight. PD, photodetector. (b) Laser beam geometry in the collimation plane. PBS, Polarizing beam splitter. $\lambda/2$, half-wave plate with slow axis tilted at α with respect to Oz. $\lambda/4$, quarter-wave plate with slow axis tilted at β with respect to Oz. The lattice beam input polarization is vertical. See text for details.

$\times 33$ kHz and $\omega_v \approx \hbar^{-1}\sqrt{16u_s\varepsilon_r/3} \approx 2\pi\times 19$ kHz for $m=0$ and $\omega_v \approx 2\pi\times 25$ kHz for $m=3$, where ε_r is the recoil energy given by $\varepsilon_r=\hbar^2k^2/(2M)$. The potential depth ΔU is given by $\hbar^{-1}\Delta U \approx \hbar^{-1}16u_s/3 \approx 2\pi\times 180$ kHz and there are approximately $\hbar^{-1}\Delta U/\omega_v \approx 8$ bound states.

Note that the vibrational frequencies are comparable with the Raman coupling $U_R \approx \hbar^{-1}u_s kl \tan(2\alpha) \approx 2\pi\times 10$ kHz where $l=\sqrt{\hbar/2M\omega_v}$ is the characteristic size of the lower vibrational state. Thus, the cooling operates in the strong Raman coupling regime and the simple physical picture of Refs. [12,19] is not applicable to our case. In particular, the Raman transitions strongly perturb the vibrational energy structure, introducing a deformation of the scalar potential. As a result, the adiabatic potentials (5), the vector term taken into account, significantly differ from the scalar potential.

IV. EXPERIMENTAL SETUP

The scheme of the experiment is represented in the diagram of Fig. 3(a). The source of the continuous beam of cold

atoms was presented in detail in [20]. It is an optical molasses loaded by a thermal cesium vapor $p=10^{-8}$ mbar. The atoms are continuously cooled and launched upwards by the moving molasses technique. We thus obtain a continuous beam of cesium atoms with a flux of the order of 10^8 at/s, a temperature between 50 and 100 μK and an adjustable velocity of about 4 m/s [20].

Collimation is carried out 22 cm above the source in a plane tilted at 3° with respect to horizontal. The geometry of the laser beams in this collimation plane is shown in Fig. 3(b). We chose a scheme suggested by Rauschenbeutel *et al.* [21] to obtain a 2D optical lattice which is intrinsically stable[1] while recycling the light to have the highest intensity. Note that, as mentioned in [21], the stability of the optical lattice is obvious if we consider it as a folded 1D lattice intersecting with itself. All four lattice beams are linearly polarized. The half-wave plate located after the beam splitter tilts the polarization by 2α with respect to its initial direction *Oz*. The quarter-wave plate, with $\beta=0$, reverses the polarization of the retroreflected beam to -2α. The pumping beam and the magnetic field direction are also in the collimation plane. The pumping beam makes a 5° angle with respect to the *Oy* lattice beam (this is imposed by the access to the vacuum system). The magnetic field which determines the quantization axis is essentially along *Oy*. A small *Ox* component (approximately 10%) is added to adjust the π polarization content of the pumping beam which is almost entirely σ^+. Finally, the pumping beam ellipticity is optimized to cancel the σ^- component. Indeed a small σ^- component leads to heating cycles, the opposite of a cooling cycle; see Fig. 1. The effect of this last adjustment on the π polarization component is negligible.

The optical lattice laser is locked to the $F=4\rightarrow F'$ manifold, which gives a detuning of 9 GHz to the red side of the $F=3\rightarrow F'$ manifold. It is a Gaussian beam of waist $w=5.68$ mm, truncated at a radius of $r=9$ mm, with a maximum power of 190 mW. The pumping beam has the same geometrical characteristics, with a typical power of about 0.6 mW. It is locked a few megahertz to the blue side of the $F=3\rightarrow F'=2$ transition.

After collimation, the atoms accomplish a parabolic flight of 0.57 s before reaching the detection region. We detect the atomic flux by fluorescence using a retroreflected probe laser beam propagating along the *Oy* direction. This beam has a diameter of 2 mm, an intensity near saturation, and is locked on the $F=4\rightarrow F'=5$ cycling transition. A repumper locked on $F=3\rightarrow F'=4$ allows us to determine the number of atoms in both $F=3$ and $F=4$ ground hyperfine states.

We measure separately the longitudinal and transverse temperatures of the atomic beam after collimation. To this end, we make use of the ballistic flight between the collimation and detection. To determine the longitudinal temperature, we proceed as follows. Just before collimation, we chop the continuous atomic beam using a pulsed transverse pushing laser beam, to produce a pulsed atomic beam with a pulse width of 5 ms. We then measure the time-of-flight distribution at detection. To determine the transverse temperature, we measure the atomic beam profile in the detection region. For this purpose, we have mounted the detection system as a whole (probe beam, collimation lens, and detector) on a translation stage in such a way that its sensitivity is independent of *x*. Note that the initial atomic beam size, probe beam size, and longitudinal temperature all affect the atomic beam profile at detection. We subtract these contributions when calculating the transverse temperature. The detection system has been calibrated to measure the atomic flux density as a function of position. In the experimental curves, we have reported the flux density measured in the detection region, at the center of the atomic beam.

V. EXPERIMENTAL RESULTS

The presence of a dark state and the strong interplay between magnetic field and pumping beam polarization are characteristic features of degenerate Raman sideband cooling. We started our study by identifying situations where sideband cooling takes place. We proceeded as follows. For different magnetic field configurations and pumper polarizations, we scanned the pumper laser frequency and recorded the fluorescence signal at detection in the center of the atomic beam. Representative results are presented in Fig. 4. On these graphs, collimation manifests itself as a positive peak. It should be noted that there is no direct correlation between the size of the peak and the transverse temperature; i.e., a very high peak does not imply a very low temperature and nor does a dip imply a high temperature (this will be clarified later). The peaks help us to identify interesting frequencies to which we then lock the pumping laser to measure the transverse temperature.

The first situation we investigated is the configuration described in Sec. II; i.e., the pumper polarization is σ^+ and the magnetic field is nearly parallel with the pumper wave vector. The result is presented in graph (a) of Fig. 4. We observe collimation due to sideband cooling on both $F=3\rightarrow F'=2$ and $F=3\rightarrow F'=3$ transitions but not on $F=3\rightarrow F'=4$. That is consistent with the fact that there is one dark state $|F=3, m_F=3, 0\rangle$ when the laser is locked to either of the former two transitions[2] but no dark state with the latter. Note also that the $32'$ peak is higher than the $33'$ peak and this can be explained as follows. The main reason is that the $F=3\rightarrow F'=3$ transition is open, and atoms spend part of their time in the $F=4$ hyperfine ground state where they experience heating due to the lattice field as becomes obvious at higher pumper intensity; see Fig. 5 and discussion below. Another effect is that some atoms may be pushed transversely out of the lattice volume by the unbalanced radiation pressure from the pumping beam before they are trapped in the potential wells.

[1]The lattice is intrinsically stable if the only effect of a phase shift of one of the laser beams, due, for example, to the vibration of a mirror, is to translate the optical lattice.

[2]On the $F=3\rightarrow F'=3$ transition, the state $|F=3, m_F=3, 0\rangle$ is dark only if the pumper polarization is purely σ^+. In practice, we adjust the magnetic field *Ox* component to cancel any π polarization.

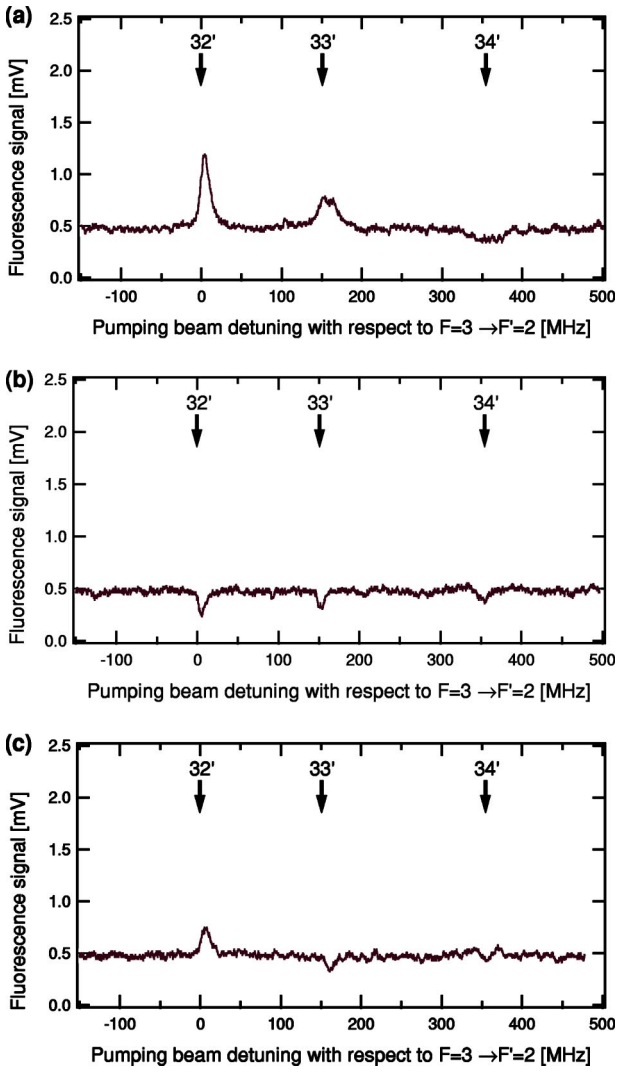

FIG. 4. Fluorescence signal detected in the center of the atomic beam as a function of pumping beam frequency. We scan over all $F=3\rightarrow F'$ transitions of the cesium D_2 line in 20 s. We investigated three different polarization configurations for the pumping laser beam. In graph (a) we adopted the configuration described in Sec. II; the pumper polarization is σ^+ and **B** is nearly parallel to the pumper, $B=150$ mG. In graph (b) we changed the pumper polarization to linear along Oz but **B** is kept nearly parallel to the pumper. In graph (c) the pumper polarization is still linear parallel to Oz and **B** is also parallel to Oz, $B=200$ mG. Other common conditions: $\alpha=22.5°$, optical lattice locked on $F=4\rightarrow F'=4$, lattice power 190 mW, and pump power 20 μW. For frequency calibration, we used saturated absorption spectroscopy.

The next situation considered is when the pumping beam polarization is linear along Oz and the magnetic field is nearly parallel with the pumping beam (Oy). In this case, the pumper is composed of both σ^+ and σ^- polarization components, so there are no dark states and we do not expect any collimation due to sideband cooling. The experimental results are displayed in graph (b) of Fig. 4. As expected, there are no collimation peaks; quite to the contrary, we observe small dips on each of the $F=3\rightarrow F'$ transitions. This can be explained because, in the presence of σ^- pumping light, we expect to observe heating, rather than cooling, cycles.

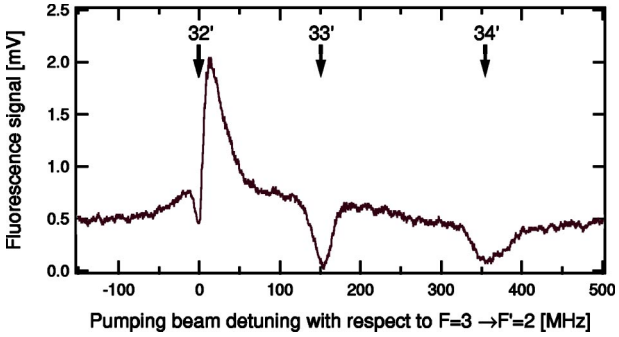

FIG. 5. Fluorescence signal detected in the center of the atomic beam as a function of pumping beam frequency. We scan over all $F=3\rightarrow F'$ transitions of the cesium D_2 line in 20 s. The polarization of the pumping beam is σ^+ and **B** is nearly parallel to the pumper, as described in Sec. II. Other conditions: $\alpha=22.5°$, optical lattice locked on $F=4\rightarrow F'=4$, $B=60$ mG, lattice power 190 mW per beam, and pump power 0.6 mW. For frequency calibration, we used saturated absorption spectroscopy.

The last situation is when the pumping beam polarization is linear along Oz and the magnetic field is also along Oz. This case corresponds to π pumping. Under the combined effect of degenerate Raman coupling and optical pumping, there is only one possible dark state: namely, when the pumping beam frequency is on the $F=3\rightarrow F'=2$ transition. This dark state is $|F=3,\ m_F=+3,\ n=0\rangle$ if $B_z>0$ and $|F=3,\ m_F=-3,\ n=0\rangle$ if $B_z<0$. The experimental results are displayed in graph (c) of Fig. 4. As expected there is a collimation peak on the $F=3\rightarrow F'=2$ transition but none on the other transitions.

The three graphs of Fig. 4 were obtained with the lowest possible pumping beam power (20 μW) in order to highlight Zeeman pumping effects in the $F=3$ ground state while limiting the effect of unwanted hyperfine pumping to the $F=4$ ground state. However, to observe efficient sideband cooling we have to increase the pumping beam intensity. Therefore we repeated the measurement of Fig. 4(a) with a higher pumping beam power (0.6 mW) and the results are presented in Fig. 5. On the two hyperfine pumping transitions ($F=3\rightarrow F'=3,4$) we observe large dips because atoms spend more time in the $F=4$ hyperfine ground state where they are heated by the strong lattice light. The $34'$ dip is wider than the $33'$ dip because of the power broadening induced by the lattice laser which is locked to the $F=4\rightarrow F'=4$ transition. We observe a very strong sideband cooling peak on the blue side of the $F=3\rightarrow F'=2$ transition, as well as a narrow dip on the red side. Note that the dip is due to heating cycles, but this will be explained in more detail later in this section.

From now on we shall focus on the first situation (pumper polarization σ^+ and magnetic field nearly parallel with the pumper as described in Sec. II) where we observe efficient sideband cooling for the pumping laser on the blue side of $F=3\rightarrow F'=2$ transition; see Fig. 5. In this situation we have searched for the laser parameters and the magnetic field that optimize atomic flux and transverse temperature.

We start with magnetic field. The theoretical value which optimizes the cooling process is such that the shift between

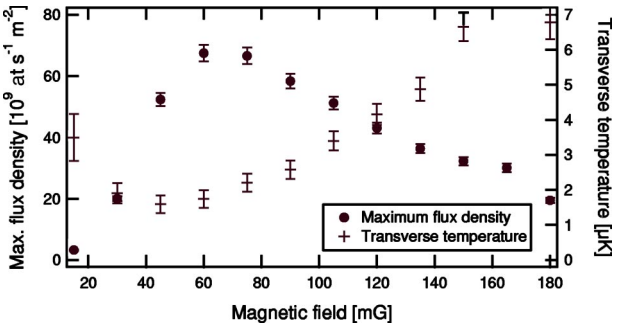

FIG. 6. Atomic flux density and transverse temperature as a function of magnetic field along Oy. The flux density is measured in the center of the atomic beam where it reaches its maximum value. Experimental conditions: $\alpha = 22.5°$, lattice locked on $F=4 \rightarrow F'=4$ transition, pumping beam locked a few megahertz above the $F=3 \rightarrow F'=2$ transition, lattice power 190 mW per beam, and pump power 0.6 mW.

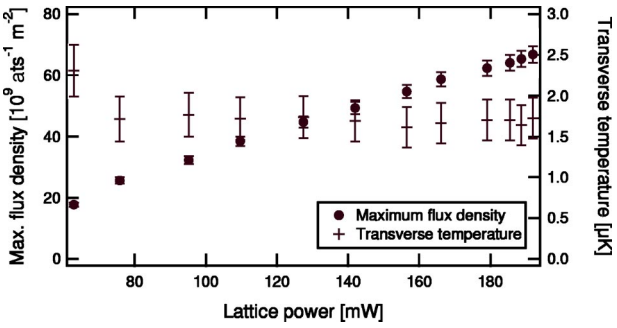

FIG. 7. Atomic flux density and transverse temperature as a function of lattice beam power. The flux density is measured in the center of the atomic beam where it reaches its maximum value. The intensity in the center of the lattice beam can be deduced from the power by $I_{\max}\ [\mathrm{mW/cm^2}] \approx 2P\ [\mathrm{mW}]$ because the beam is Gaussian with a waist $w = 5.68$ mm. Same experimental conditions as in Fig. 6 but with $B = 60$ mG.

adjacent Zeeman sublevels equals the vibrational level spacing in the lattice wells. However, in our experiment, a continuous atomic beam crosses a combination of Gaussian laser beams, leading to position- and time-dependent well depth and vibrational frequencies ω_v. The time dependence satisfies the adiabaticity condition $1/\omega_v \times d\omega_v/dt \ll \omega_v$ but the magnetic tuning condition can only be met in an average sense and if the vibration levels are sufficiently broadened by the pumping light. We have measured the transverse temperature and atomic flux density as a function of magnetic field amplitude. Results are shown in Fig. 6. We find that the temperature is minimum for $B = 50$ mG and the atomic flux density is maximum for $B = 60$ mG.

We have repeated this measurement for values of α ranging from 0° to 45°. Let us recall that the lattice beam polarization is linear and tilted from the Oz axis by $+(-)2\alpha$ for the forward (retroreflected) beam. For $2\alpha = 0°$ the flux practically vanishes, together with the Raman transition probability. The flux then increases with tilt angle, reaches a maximum at $2\alpha = 45°$, and decreases again. The dependence of the transverse temperature as a function of magnetic field is the same for all values of α.

The effect of lattice laser intensity is shown in Fig. 7. The atomic flux grows steadily with lattice beam intensity. There is no obvious sign of saturation and the transverse temperature is nearly constant. Note that we kept the magnetic field at a fixed value even if it can be expected that the optimum magnetic field changes with the lattice intensity. This should not change the result to a significant degree because the expected variation of the optimum magnetic field is less than 40% and the resonance in B is smooth in this range.

We have also repeated our flux and temperature measurements for various values of the lattice laser frequency by locking it to each of the three $F=4 \rightarrow F'$ transitions and their crossovers. We observed no difference except for the $F=4 \rightarrow F'=5$ transition frequency, for which the atomic flux vanishes. This result is easily understandable: for all transitions and with sufficient intensity, the lattice laser also acts as a repumper to the $F=3$ level, except when it is tuned to the cycling, $F=4 \rightarrow F'=5$, transition.

The cooling efficiency is much more critically dependent on the pumping laser frequency, however. This effect can be expected from the size and sign of the light shifts experienced by the different Zeeman sublevels of the $F=3$ state, as observed and explained by Kerman *et al.* [15]. Because of the σ^+ polarization of the pumping beam, the $F=3$, $m_F=1$ sublevel is shifted, but the $F=3$, $m_F=2$ and $F=3$, $m_F=3$ sublevels are not as they are dark to the σ^+ pumper light. If the light shift is negative, which is the case for a red detuning, it will lead to a heating, instead of a cooling, cycle if the light shift is comparable with the Zeeman shift. This argument explains the dip observed in Fig. 5 and the fact that the cooling efficiency is much higher on the blue side than on the red side of the $F=3 \rightarrow F'=2$ transition. This behavior is indeed observed in Fig. 8. Notice that the temperature is lower on the red side. This can be explained because all atoms not in the dark state $|F=3,\ m_F=3,\ 0\rangle$ are lost by heating. Thus, only a small fraction of very cold atoms remains.

VI. DISCUSSION

A. Optimum magnetic field

The dependence of flux and temperature on magnetic field (see Fig. 6) is characteristic of Zeeman-shift degenerate-

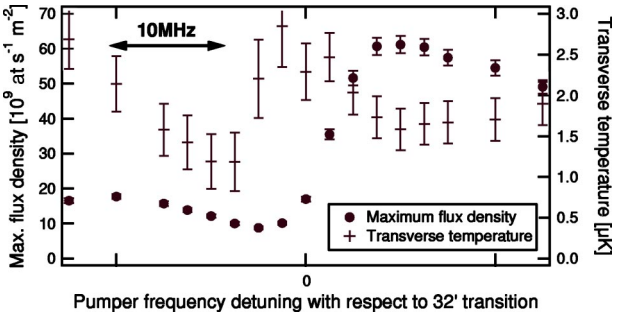

FIG. 8. Atomic flux density and transverse temperature as a function of pumping laser frequency, in a range of a few tens of megahertz around the $F=3 \rightarrow F'=2$ transition of the Cs D_2 line. The flux density is measured in the center of the atomic beam where it reaches its maximum value. Same experimental conditions as in Fig. 6 but with $B = 60$ mG.

Raman-sideband cooling. Due to the Gaussian profile of the laser beams, the resonance is smeared out, but there is a clear optimum of temperature when $B \approx 50$ mG. In order to compare this value with theory, we have calculated the optical potential wells and the vibrational frequencies corresponding to our experimental conditions. In the center of the laser beam, we have $I = 380$ mW cm^{-2}; thus, we obtain $\omega_v \approx 2\pi \times 50$ kHz. At the edge of the laser beam ($r = 9$ mm), we have $I = 2.5$ mW cm^{-2}, corresponding to $\omega_v \approx 2\pi \times 4$ kHz. The magnetic field necessary to shift adjacent Zeeman sublevels by an amount equal to the vibrational energy splitting is $B_{\max} \approx 140$ mG in the center and $B_{\min} \approx 11$ mG at the edge of the laser beam.[3] The experimental optimum lies between these upper and lower bounds.

B. Adiabatic cooling

Due to the Gaussian shape of laser beams, atoms should undergo an adiabatic expansion while leaving the cooling zone and this should reduce the temperature [15–17]. To check if this adiabatic cooling takes place in our experiment we have masked the upper part (approximately 25%) of the laser beams and we made the following observations. When we blocked the upper part of all laser beams (lattice and pump) the temperature increased by a few tens of microkelvin. This could lead us to believe that there is adiabatic cooling. However, we repeated the experiment, masking only the top of the pumping beam, and the temperature increased even more (although adiabatic expansion should still take place). We deduce that, after having crossed three-quarters of the cooling zone, only a small fraction of atoms have reached the dark state $|F=3,\ m_F=3,\ n=0\rangle$ and for this reason the effect of adiabatic cooling is imperceptible. This also means that in the future, we might be able to lower the temperature by increasing the size of laser beams and therefore the transit time of atoms in the cooling zone.

C. Final temperature

Without adiabatic cooling, the final temperature is linked to the kinetic energy of atoms inside the optical lattice and, thus, to the average vibrational frequency. We can calculate the vibrational ground-state kinetic temperature using $\frac{1}{2}k_B T_0 = \langle E_{\text{kinetic}} \rangle = \frac{1}{4}\hbar\omega_v$. For $I = 100$ mW cm^{-2} we have $\omega_v \approx 2\pi \times 25$ kHz and thus $T_0 = 0.6$ μK. This is the lowest possible final temperature which is reached if all atoms are in the vibrational ground state. However, in the strong coupling regime, one cannot expect the final vibrational ground-state population to be close to 1, because of the competition between off-resonant and resonant Raman transitions (see also Sec. VI E). Moreover, the spatial and temporal inhomogeneity of the optical lattice parameters prevent the resonance condition $\Delta E_{\text{Zeeman}} = \hbar\omega_v$ from being fulfilled everywhere. This further reduces the final population of the ground state and thus increases the final temperature. As a result, we expect an average vibrational number between 0.5 and 1 which corresponds to a final temperature between 1.2 and 1.8 μK.

[3]The Zeeman frequency shift of adjacent magnetic sublevels is 350 kHz/G for the hyperfine ground states of cesium.

D. Cooling of unbound atoms in far-detuned optical lattice

One important ingredient of the sideband-resolved Raman cooling scheme of Hamann *et al.* [12] is an effective loading of atoms into a few lower vibrational levels. For this purpose, they used the polarization-gradient cooling in a near-resonant optical lattice. In the method of Treutlein *et al.* [16] the precooling stage is absent, and the results obtained in [16] suggest that two (probably different) cooling mechanisms coexist: one for tightly bound atoms in the Lamb-Dicke regime and another for unbound atoms moving above the optical lattice potential. The experiments presented here correspond, in principle, to the method of Treutlein *et al.*, but with much higher temperature. In order to ensure that unbound atoms are actually cooled in the present scheme, we have started to consider this problem in the framework of the standard semiclassical approach [22–30]. Namely, following the work in Ref. [31], we have developed analytical expressions for the local friction $\mathcal{X}$ and diffusion $\mathcal{D}$ coefficients in the case of a model $1 \rightarrow 0$ transition. The stationary temperature of unbound atoms is estimated as $k_B T = -\langle \mathcal{D} \rangle / \langle \mathcal{X} \rangle$, where the angular brackets denote spatial averaging over the lattice period. We perform numerical averaging of the friction and diffusion for a 1D model configuration. The dependences on parameters (pumper detuning, Zeeman shift, lattice intensity, etc.) we have obtained reproduce the main qualitative features of the experimental results.

Note that, from the semiclassical point of view employed here, we are dealing with a new kind of polarization-gradient cooling where the atomic recoil is provided by stimulated rescattering of far-detuned photons in a nondissipative optical lattice, while the near-resonant optical pumping plays the role of an effective relaxation in the system. Both Doppler-like and Sisyphus-like cooling are possible, depending on the angular momenta of the levels, pumping field polarization, and other parameters. A detailed theoretical study will be communicated elsewhere.

E. Model of sideband Raman cooling in the Lamb-Dicke regime

Reference [19] describes a model of degenerate-Raman-sideband cooling in a case where the adjacent Zeeman states are displaced by the Stark shift of an auxiliary laser beam. By adapting the method described therein, we have performed numerical calculations of the steady-state distribution among the Zeeman and vibrational substates for a model $1 \rightarrow 0$ transition. We took into account five vibrational states for each Zeeman sublevel and all possible Raman transitions. We studied a model 1D lattice formed by linearly polarized counterpropagating laser beams in lin-θ-lin configuration with a magnetic field orthogonal to the beam directions. In this lattice, the ratio U_R/ω_v is controlled by both the angle θ and the lattice intensity. The results for the average vibrational excitation number are shown in Fig. 9. As can be seen, they are in qualitative agreement with the experimentally observed dependence; see Fig. 6.

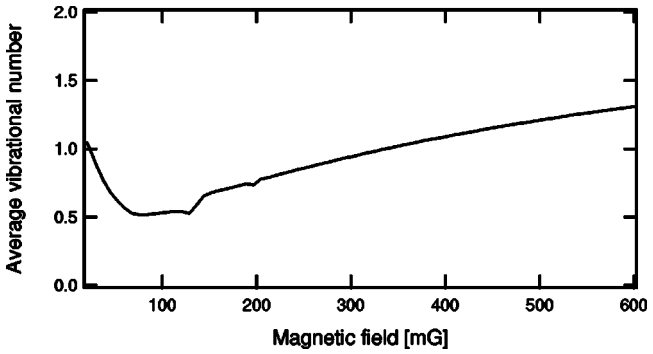

FIG. 9. Average vibrational number as a function of magnetic field. Parameters used in numerical calculations: vibrational frequency $\omega_v = 2\pi \times 19$ kHz, Raman transition rate $\hbar^{-1}U_R = 2\pi \times 11$ kHz, pumping field intensity 0.1 mW cm^{-2}, and detuning +2.6 MHz.

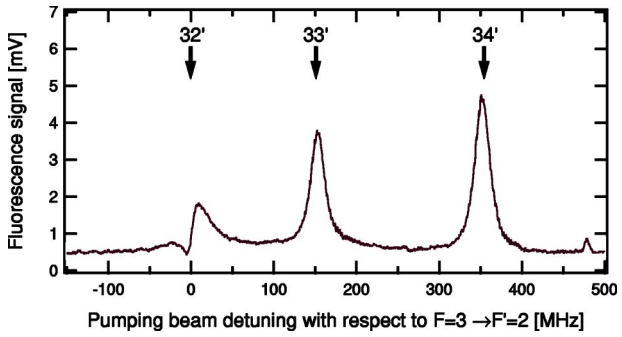

FIG. 10. Fluorescence signal detected in the center of the atomic beam as a function of pumping beam frequency. We scan over all the $F=3 \rightarrow F'$ transitions of the cesium D_2 line in 20 s. Same conditions as in Fig. 6 but we locked the lattice on the red side of $F=4 \rightarrow F'=5$ transition with a detuning of 126 MHz. For frequency calibration, we used saturated absorption spectroscopy. See Sec. VI G for comments.

F. Comparison with Sisyphus cooling

To evaluate the efficiency of sideband cooling, it is interesting to compare it with Sisyphus cooling in the same geometry. When $\alpha = 22.5°$ the optical lattice has the same geometry as a 2D lin $\perp$ lin molasses. Therefore we just have to lock the lattice on the red side of the $F=4 \rightarrow F'=5$ transition and the pumper on the $F=3 \rightarrow F'=4$ transition to produce the conditions for Sisyphus cooling. The atomic flux and transverse temperatures obtained after optimization of all parameters are presented in Table I. The flux is weaker with sideband than with Sisyphus cooling. This is most probably due to the very high temperature (≈ 60 μK) of atoms when they enter the optical lattice. The question of how to increase the flux is discussed in the next subsection.

G. Possibility to increase the flux

To push up the intensity of the atomic beam, we would need an efficient precooling mechanism, preferably superimposed with the optical lattice [12]. With this in mind, we locked the lattice laser 126 MHz below the $F=4 \rightarrow F'=5$ resonance and scanned the pumping laser frequency over all $F=3 \rightarrow F'$ transitions of the D_2 line. The result is reported in Fig. 10. This graph deserves several comments. First, we observe degenerate-Raman-sideband cooling on the $F=3 \rightarrow F'=2$ transition as described in Sec. V, Fig. 8. Second, we observe two big cooling peaks on the $F=3 \rightarrow F'=3$ and the $F=3 \rightarrow F'=4$ transitions. We measured the transverse temperature of these peaks and obtained approximately 20 μK. Here the atoms are distributed equally in both hyperfine ground states whereas for sideband cooling they are all in $F=3$. Moreover, the peaks disappear when $\alpha = 0$—i.e., without polarization gradients. Therefore these peaks are consistent with a Sisyphus-like polarization gradient cooling mechanism.

This graph (Fig. 10) shows that two complementary cooling mechanisms can coexist in the same lattice, each corresponding to a different pumping beam frequency. Thus, it seems possible to combine the high efficiency of Sisyphus-like cooling with the low temperature of sideband cooling in the same lattice beams: a first zone, where Sisyphus precooling would be achieved with a pumper tuned to the $F=3 \rightarrow F'=4$ transition, would be followed by a second zone where another pumper, tuned to the $F=3 \rightarrow F'=2$ transition, would achieve sideband cooling. We expect this second step to be much more efficient because it would start at a much lower temperature than that used up to now: namely, a few microkelvins instead of 60 μK.

Figure 10 deserves one last comment: we observe a small structure 125 MHz above the $F=3 \rightarrow F'=4$ transition. We have observed the same peak in other situations and found it is always located at $\nu_{\text{pump}} = \nu_{\text{lattice}} + 9.2$ GHz—i.e., when the frequency difference between the two lasers coincides with the ground-level hyperfine splitting. It has not yet been investigated.

TABLE I. Comparison of sideband and Sisyphus cooling mechanisms *in optimized conditions*, as discussed in Sect. VI F. The flux density is measured, after a parabolic flight of 0.57 s, in the center of the atomic beam. The sideband conditions are $B=60$ mG, $\alpha = 22.5°$, optical lattice locked on $F=4 \rightarrow F'=4$, pumper locked a few megahertz on the blue side of the $F=3 \rightarrow F'=2$ transition, lattice power 190 mW, and pump power 0.6 mW. The Sisyphus conditions are $B=0$, $\alpha = 22.5°$, lattice locked on the red side of $F=4 \rightarrow F'=5$ transition with a detuning of 126 MHz, pumper locked on the $F=3 \rightarrow F'=4$ transition, lattice power 16 mW, and pump power 0.1 mW.

Cooling mechanism	Transverse temperature (μK)	Atomic flux density (at. s^{-1} m^{-2})
Sideband	1.6	7×10^{10}
Sisyphus	3.6	3.6×10^{11}

VII. CONCLUSION

Our experiment provides a demonstration of degenerate-Raman-sideband cooling for the collimation of a continuous beam of cold cesium atoms. Starting from an initial trans-

verse temperature of 60 μK, we obtained final transverse temperatures as low as 1.6 μK in a single-laser interaction zone. The total flux of 10^7 at./s corresponds to an efficiency of approximately 10%. We have also identified another, Sisyphus-like, cooling mechanism which requires a different pumper frequency in the same lattice. This provides nearly 100% efficiency, but with a higher final temperature. Our 2D four-beam optical lattice combines intrinsic phase stability, symmetry, and power recycling. In addition, all laser beams are in a plane perpendicular to the atomic beam, a practical advantage in view of expected applications such as atomic fountain clocks, atom interferometers, and atom optics experiments. We have started theoretical studies of laser cooling in a lattice in the strong Raman coupling regime, both for bound and unbound atoms. Preliminary results with a 1D model of Raman sideband cooling are verified by our experimental data.

Two main avenues for improvement are being explored. First, we plan to combine the high capture efficiency of Sisyphus-like cooling with the low temperature of Raman sideband cooling by implementing them consecutively in the same optical lattice. Second, we intend to replace Zeeman tuning by ac Stark tuning as described in Ref. [19]. For cold atomic fountain clocks, this has the significant advantage of preparing all atoms in one of the clock states (m_F=0).

ACKNOWLEDGMENTS

We would like to thank C. Affolderbach and M.D. Plimmer for a careful reading of the manuscript. This work was supported by the Swiss National Science Foundation, the Swiss Federal Office of Metrology and Accreditation (METAS), the canton of Neuchâtel, and the Swiss Confederation. A.V.T. and V.I.Y. were partially supported by Grant No. INTAS-01-0855 and by RFBR through Grant Nos. 04-02-16428, 04-02-16488, and 04-02-16525.

[1] H. J. Metcalf and P. van der Straten, *Laser Cooling and Trapping* (Springer, Berlin, 1999).
[2] P. R. Berman, *Atom Interferometry* (Academic Press, San Diego, 1997).
[3] S. C. A. Peters and K. Y. Chung, Nature (London) **400**, 849 (1999).
[4] Y. Sortais *et al.*, Phys. Scr. **50**, 50 (2001).
[5] A. Joyet, G. Mileti, P. Thomann, and G. Dudle, in *Proceedings of the Sixth Symposium on Frequency Standards and Metrology*, edited by P. Gill (World Scientific, Singapore, 2002).
[6] Special issue on the Dick effect, edited by L. Maleki, IEEE Trans. Ultrason. Ferroelectr. Freq. Control **45**(4), 876 (1998).
[7] A. Joyet, G. Mileti, G. Dudle, and P. Thomann, IEEE Trans. Instrum. Meas. **50**, 150 (2001).
[8] D. J. Wineland and H. Dehmelt, Bull. Am. Phys. Soc. **20**, 637 (1975).
[9] F. Diedrich, J. C. Bergquist, W. M. Itano, and D. J. Wineland, Phys. Rev. Lett. **62**, 403 (1989).
[10] D. J. Heinzen and D. J. Wineland, Phys. Rev. A **42**, 2977 (1990).
[11] R. Taïeb, R. Dum, J. I. Cirac, P. Marte, and P. Zoller, Phys. Rev. A **49**, 4876 (1994).
[12] S. E. Hamann, D. L. Haycock, G. Klose, P. H. Pax, I. H. Deutsch, and P. S. Jessen, Phys. Rev. Lett. **80**, 4149 (1998).
[13] H. Perrin, A. Kuhn, I. Bouchoule, and C. Salomon, Europhys. Lett. **42**, 395 (1998).
[14] V. Vuletic, C. Chin, A. J. Kerman, and S. Chu, Phys. Rev. Lett. **81**, 5768 (1998).
[15] A. J. Kerman, V. Vuletic, C. Chin, and S. Chu, Phys. Rev. Lett. **84**, 439 (2000).
[16] P. Treutlein, K. Y. Chung, and S. Chu, Phys. Rev. A **63**, 051401(R) (2001).
[17] A. Kastberg, W. D. Phillips, S. L. Rolston, R. J. C. Spreeuw, and P. S. Jessen, Phys. Rev. Lett. **74**, 1542 (1995).
[18] I. H. Deutsch and P. S. Jessen, Phys. Rev. A **57**, 1972 (1998).
[19] A. V. Taichenachev, A. M. Tumaikin, V. I. Yudin, and L. Hollberg, Phys. Rev. A **63**, 033402 (2001).
[20] P. Berthoud, E. Fretel, and P. Thomann, Phys. Rev. A **60**, R4241 (1999).
[21] A. Rauschenbeutel, H. Schadwinkel, V. Gomer, and D. Meschede, Opt. Commun. **148**, 45 (1998).
[22] J. Dalibard and C. Cohen-Tannoudji, J. Opt. Soc. Am. B **6**, 2023 (1989).
[23] Y. Castin and K. Mölmer, J. Phys. B **23**, 4101 (1990).
[24] K. Mölmer, Phys. Rev. A **44**, 5820 (1991).
[25] G. Nienhuis, P. van der Straten, and S.-Q. Shang, Phys. Rev. A **44**, 462 (1991).
[26] S. M. Yoo and J. Javanainen, Phys. Rev. A **45**, 3071 (1992).
[27] V. Finkelstein, P. R. Berman, and J. Guo, Phys. Rev. A **45**, 1829 (1992).
[28] J. Werner, G. Hillenbrand, and A. Steane, J. Phys. B **26**, 3063 (1993).
[29] S. Chang, T. Y. Kwon, H. S. Lee, and V. Minogin, Phys. Rev. A **60**, 2308 (1999).
[30] S. Chang, T. Y. Kwon, H. S. Lee, and V. G. Minogin, Phys. Rev. A **64**, 013404 (2001).
[31] A. Bezverbny, O. Prudnikov, A. Taichenachev, A. Tumaikin, and V. Yudin, J. Exp. Theor. Phys. **96**, 383 (2003).